ISBN: 978-3-95450-204-2 ISSN: 2673-5350 doi:10.18429/JACoW-IBIC2019-WEPP030

BETATRON PHASE ADVANCE MEASUREMENTS USING THE GATED TURN-BY-TURN MONITORS AT SuperKEKB

G. Mitsuka*, K. Mori, M. Tobiyama, KEK, Ibaraki, Japan

Abstract

In the SuperKEKB commissioning Phases 2 (Feb.-Jul. 2018) and 3 (from Mar. 2019), the betatron phase advances between adjacent beam position monitors have been measured using a total of 138 gated turn-by-turn monitors. A fast RF gating of the monitors enables turn-by-turn beam position detection by focusing only on an artificially-excited non-colliding bunch, while leaving colliding bunches unaffected. Betatron phase advances measured by the gated turn-by-turn monitors and accordingly obtained betatron functions were consistent with the closed orbit measurements. High signal-to-noise ratio were achieved by advanced signal extraction methods such as NAFF, SVD, and independent component analysis.

INTRODUCTION

Since SuperKEKB aims at very high luminosity $8 \times 10^{35}\,\mathrm{cm}^{-2}\mathrm{s}^{-1}$, transverse beam sizes at the interaction point (IP) must be squeezed down to 10 µm and 50 nm in horizontal and vertical plane, respectively. Therefore minimization of betatron coupling (X-Y coupling) and vertical dispersion, causing an increase in beam size, is crucial at SuperKEKB. Additionally, betatron function measurements and its corrections are of importance, since a disturbance of the betatron function leads to a dynamic aperture reduction and a vertical emittance growth.

At SuperKEKB we usually estimate X-Y coupling and vertial dispersion by closed orbit analysis for a beam artificially excited by steering magnets. However, these measurements need few tens of minutes in total and are limited to be performed in low-current operation ($\lesssim$ 30 mA) with no collision to avoid an accidental system quench. Therefore, fast beam-optics measurements during beam-beam collision and/or high-current operation are desired to compensate close orbit analysis.

For measurements during collisions, we utilize the injection kickers or the transverse feedback kickers to excite a specific non-colliding bunch, while leaving colliding bunches unaffected. Electrode signals from beam position monitors (BPMs) for only a non-colliding bunch are specially processed by the gated turn-by-turn beam position monitors (GTBTs) [1]. Main purposes of the GTBTs are as follows.

- Beam optics measurements using a non-colliding bunch during beam-beam collisions and high-current operation
- Beam study such as measurements for betatron function or X-Y coupling at IP
- Beam diagnostics during beam injection

* gaku.mitsuka@kek.jp

GATED TURN-BY-TURN MONITORS

Shown in Fig. 1 is the top view of the GTBT detector circuit contained in a 1U rack-mount case. A GTBT detector has four-channel BPM inputs. Incoming BPM electrode signals first go to a fast RF gating switch [3] where signals from only a non-colliding bunch (pilot bunch) are accepted, and other bunch signals are rejected. Rejected BPM signals return to four-channel BPM outputs connecting to an external 508 MHz narrow-band detector circuit in charge of a closed orbit analysis. Accepted pilot bunch signals are processed in a GTBT by 508 MHz band pass filters, low-noise amplifiers (HMC616, total gain 40 dB), log-ratio amplifier (ADL5513), peak hold circuit, and are finally analog-digital converted by a 14 bits ADC (ADS850). Timing to control these processes is issued by the Xilinx FPGA (Spartan-6, XC6SLX100T-3FGG484).

Figure 2 indicates the RF gating response, where the one-bunch signal (bottom red) is cut from the input all-bunch signals (top blue, −20 dBm). Switching noise is suppressed to 2 mVpp. Both rise time and fall time are 0.6 ns, which are well shorter than the bunch separation (4 ns). Insertion loss

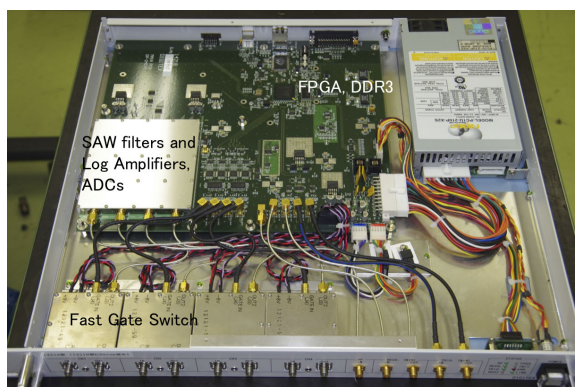

Figure 1: Top view of the GTBT detector.

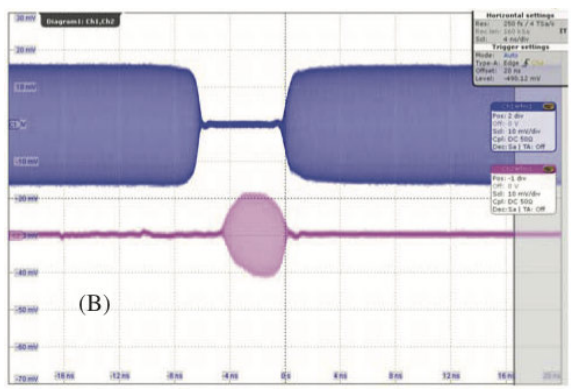

Figure 2: Switch response for a 4 ns gate input.

ISBN: 978-3-95450-204-2 ISSN: 2673-5350 doi:10.18429/JACoW-IBIC2019-WEPP030

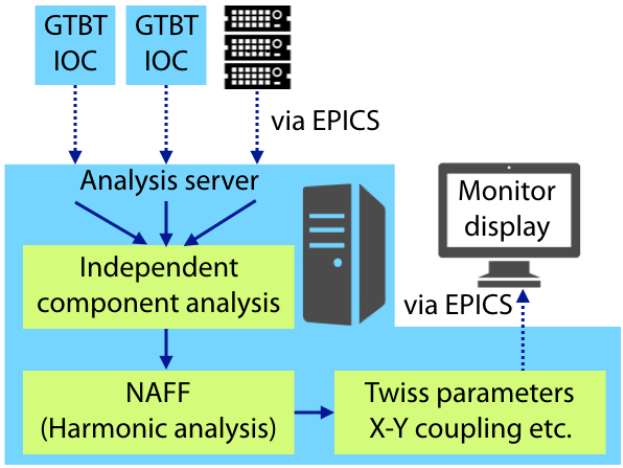

Figure 3: Data flow of the gated turn-by-turn monitors.

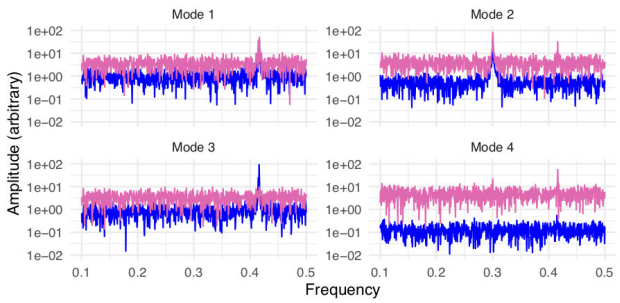

Figure 4: Frequency spectra of four decomposed components by SVD (purple) and ICA (blue).

owing to the RF gating is 4 dB and the isolation is 80 dB, both of which fully meet our requests.

Installation of the GTBTs started before the Phase 1 commissioning (Feb.-Jun. 2016) and 22 GTBTs were specially added to the interaction and injection regions before Phase 2. Currently total of 68 and 70 GTBTs are operated in e^- ring (HER) and e^+ ring (LER), respectively.

DATA FLOW AND ANALYSIS METHODS

Figure 3 summarizes the GTBT data flow and analysis methods. Total of 21 Linux servers (denoted as "GTBT IOC") dedicated to the GTBT data processing first collects the data from adjacent several GTBTs. The electrode signals proportional to Volt. are converted to a bunch position in units of mm in EPICS IOCs at these Linux servers following the pre-defined 3rd-order polynomial functions.

Betatron function is derived in a Linux analysis server, where we first make a collection of the position and timing information of all the GTBTs through EPICS IOCs. Next we apply Independent Component Analysis [4] (ICA) to the data collection. ICA decomposes the mixed data into additive sub-components (modes). The total number of decomposed modes must be predetermined before running ICA depending on data quality. At SuperKEKB, 4 to 6 modes are enough to separate the betatron oscillation and other noise components.

Here we compare the decomposition performances between ICA and the singular value decomposition (SVD). Shown in Fig. 4 are the frequency spectra of the mixed data containing the real data with a betatron oscillation at $\nu_y \sim 0.42$ and a dummy oscillation data at $\nu = 0.3$. ICA clearly separates a betatron oscillation and a dummy oscillation, while for the SVD these two oscillations are still left mixed as in the mode 2 and 4 spectra. We use ICA in the following analyses to have good noise reduction performance.

After data cleaning by ICA, we perform a harmonic analysis to determine a fundamental frequency (tune), phase, and amplitude. For the harmonic analysis in this study, we use NAFF [5] instead of fast Fourier transform (FFT). Figure 5 compares the determination resolution of frequency, amplitude, and phase as a function of the number of turns to be analyzed. Test data intendedly contains random noise data generated following a normal distribution, as well as a signal sinusoidal wave with a fixed frequency, amplitude, and phase. The noise-to-signal ratio is set to 10 %. As seen in Fig. 5, NAFF has a better resolution than FFT for all variables and reaches sufficient performance at around 1000 turns. Good enough resolution at $\mathcal{O}(10^2)$ turns is of great advantage for beam injection tuning usually performed with the limited number of turns. A decrease in an oscillation amplitude throughout the data due to radiation dumping can also be minimized as the number of turns gets smaller.

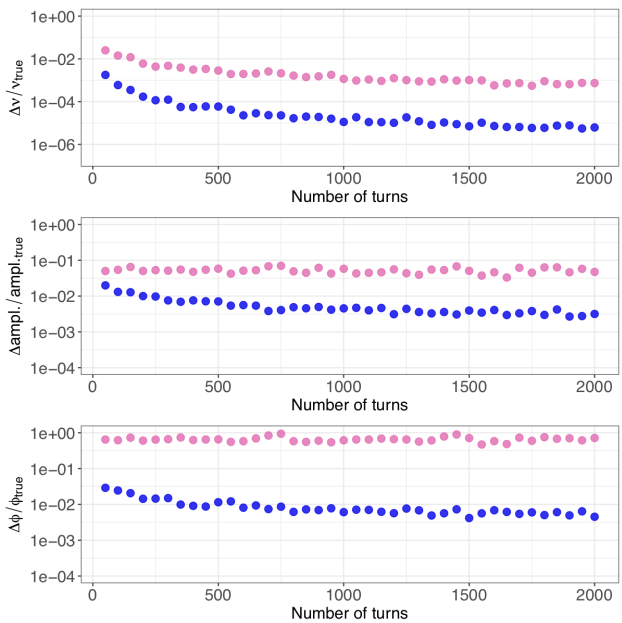

Figure 5: (Top) Frequency, (middle) amplitude, and (bottom) phase measurements by FFT (purple filled circles) and NAFF (blue filled circles).

ISBN: 978-3-95450-204-2 ISSN: 2673-5350 doi:10.18429/JACoW-IBIC2019-WEPP030

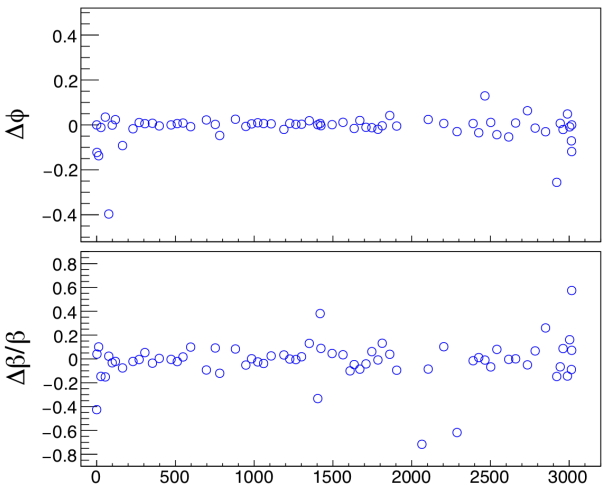

Figure 6: (Top) Phase advance and (bottom) beta-beat measurements in the SuperKEKB electron ring in Phase 3.

BETATRON FUNCTION MEASUREMENTS

Betatron function is derived using the phases and amplitudes determined by NAFF. Figure 6 indicates residual in a phase advance defined as $\Delta\phi \equiv \phi_{\mathrm{GTBT}} - \phi_{\mathrm{SAD}}$ (top panel), and a beta beat defined as $\Delta\beta/\beta \equiv (\beta_{\mathrm{GTBT}} - \beta_{\mathrm{SAD}})/\beta_{\mathrm{SAD}}$ (bottom panel). In the both panels, the GTBT measurements are compared with the SAD model predictions. The GTBT data was taken in Phase 3 as horizontally exciting a non-colliding bunch by the injection kicker. Standard deviations are $\sigma_{\Delta\phi} = 0.07$ and $\sigma_{\Delta\beta/\beta} = 0.17$ for a phase advance and a beta beat, respectively.

Regarding the phase advance, sizable disagreements between the GTBT data and the SAD model prediction are found near the IP (0 m or 3016 m). This tendency is also seen in a comparison of the closed orbit analysis with the SAD model prediction, thus is expected to owe to possible residual of the SAD modeling.

For the betatron function, we find disagreements between the GTBT data and the SAD model prediction near the IP similarly with the phase advance. They are clearly propagated from the phase disagreements found in the top panel. Here we should note that in this study the betatron function is obtained using the oscillation amplitude which is unavoidably sensitive to the GTBT absolute gain calibration. The betatron function calculated by the 3BPM method [6], using adjacent three BPMs' phase advance instead of their amplitudes, provides an overall good agreement with the SAD model prediction. The standard deviations $\sigma_{\Delta\phi}$ and $\sigma_{\Delta\beta/\beta}$ of the closed orbit analysis relative to the SAD model prediction are about 1/3 of those found in Fig. 6.

X-Y COUPLING AT THE IP

Figure 7 indicates the specific luminosity ($\mathrm{cm^{-2}\,s^{-1}/mA^2}$) as a function of the beam current product ($\mathrm{mA^2}$) in Phase 2 [7], whereas in Fig. 8 the simulated specific luminosity as a function of the beam current product indicates how specific luminosity degrades owing to finite chromatic X-Y coupling at the IP [8]. Defining $x\cdots$ as coupled coordinates and $X\cdots$ as decoupled coordinates, these two coordinates can be expressed as

$$\begin{pmatrix} x \\ x' \\ y \\ y' \end{pmatrix} = \begin{pmatrix} \mu & 0 & r_4 & -r_2 \\ 0 & \mu & -r_3 & r_1 \\ -r_1 & -r_2 & \mu & 0 \\ -r_3 & -r_4 & 0 & \mu \end{pmatrix} \begin{pmatrix} X \\ X' \\ Y \\ Y' \end{pmatrix}, \qquad (1)$$

where r_i are the coupling parameters and $\mu^2 + (r_1 r_4 - r_2 r_3) = 1$. According to the simulation results in Fig. 8, chromatic components of X-Y coupling $r_1' \sim 12$ rad and $r_2' \sim 3$ m are potential sources of specific luminosity degradation seen in Fig. 7.

The r_3' and r_4' values considered in the simulation are far large compared with the GTBT measurements discussed below. Therefore measured amounts of r_3' and r_4' are expected to have only sub-leading effects to the specific luminosity. Discussion here is based on the Phase 2 results, nevertheless, since specific luminosity degradation is foreseen in Phase 3, we analyze the chromatic components of X-Y coupling at the IP using GTBTs in Phase 3.

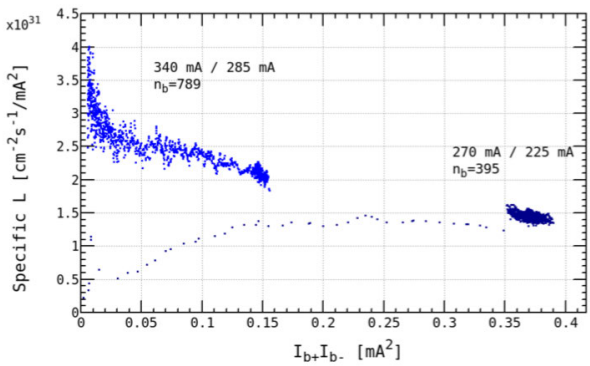

Figure 7: Specific luminosity for each beam current product in Phase 2.

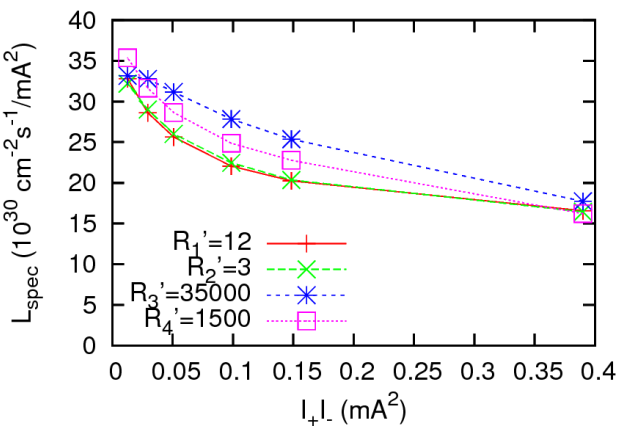

Figure 8: Simulated specific luminosity degradation for each chromatic coupling parameter.

ISBN: 978-3-95450-204-2 ISSN: 2673-5350 doi:10.18429/JACoW-IBIC2019-WEPP030

Shown in Fig. 9 are the X-Y coupling parameters in LER at the IP for each $\Delta p/p$. Filled red circles indicate the GTBT data taken in Phase 3, blue solid curves indicate the bestfit 2nd-order polynomial functions, and gray filled area indicate 68 % confidence intervals. Fitting a 2nd-order polynomial function

$$r_i \equiv r_i^0 + r_i^{'}\left(\frac{\Delta p}{p}\right) + r_i^{''}\left(\frac{\Delta p}{p}\right)^2$$

to r_i obtained by the GTBT data at each $\Delta p/p$ gives the bestfit $r_1^{'} - r_4^{'}$ values. As seen in the upper left and right panels in Fig. 9, $r_1^{'} = 3.32 \pm 1.36$ rad and $r_2^{'} = 1.15 \pm 0.29$ m were obtained, respectively. These values correspond to about 30–40 % of the simulation in Fig. 8.

Next we compare the GTBT results with another measurement result called "beam-beam scan". In the beam-beam scan method, $r_1^{'}$ can be obtained by evaluating the changes in the vertical beam size at the IP for each $\Delta p/p$. The $r_1^{'}$ value by the beam-beam scan method resulted in about 50 % of the simulation in Fig. 8; the measured change was $\Delta\sigma^{\star}_{y,\mathrm{meas}} = 0.26\,\mu$m, while the simulation predicted $\Delta\sigma^{\star}_{y,\mathrm{sim}} = 0.55\,\mu$m for $r_1^{'} = 12$ rad. According to the fact that the $r_1^{'}$ values obtained by GTBT and the beam-beam scan are comparable considering statistical uncertainties, 30–50 % of the specific luminosity degradation in Phase 3 can be explained by $r_1^{'}$.

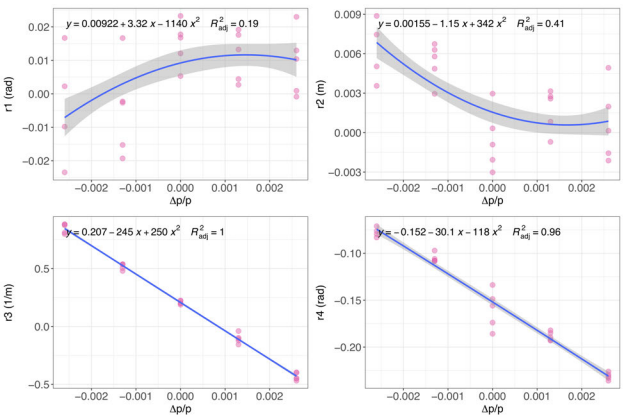

Figure 9: X-Y coupling parameters in LER in Phase 3.

R&D STATUS OF THE NEW GTBTS

As explained in the previous sections, the present GTBT system has been well functioning throughout Phase 1 to 3. Nevertheless, a mojor upgrade to the currently working GTBT detector circuit is necessary to realize high-speed data processing. Table 1 summarizes differences in the present GTBTs and upgrade strategy.

In the upgrade GTBT system, transverse beam position will be extracted from the four-channel electrode signals in the Xilinx Zynq FPGA, which significantly accelerates Volt. to mm conversion compared with the present GTBT system. Second, a harmonic analysis embedded in the Zynq FPGA enables a realtime frequency and phase determination with no latency time due to the data transfer via EPICS IOC, and thus is advantageous in the phase synchronization across all GTBTs.

Table 1: Proposed Upgrades to the Present Gated Turn-by-turn Monitor

	Present GTBT	**Upgrade GTBT**
Position calculation	EPICS IOC	Zynq
Realtime analysis	None	Zynq
TCP/IP network	SiTCP	Arm Linux

Finally, the Arm Linux is responsible in a TCP/IP connection in the upgrade GTBTs, in contrast to the SiTCP-based TCP/IP connection in the present GTBTs. R&D of the upgrade GTBTs started in 2018, and a first prototype detector will be ready for performance test at KEK by spring 2019.

REFERENCES

[1] M. Tobiyama, H. Fukuma, H. Ishii, and K. Mori, "Development of Gated Turn-by-Turn Position Monitor System for the Optics Measurement During Collision of SuperKEKB", in *Proc. IBIC2013*, Oxford, UK, Sep. 2013, paper MOPF32, pp. 295–298.

[2] H. Ishii *et al.*, "Development of a 508 MHz Narrowband Detector for Beam Position Monitors", in *Proc. PASJ2014*, Aomori, Japan, Aug. 2014, paper SUP074, pp. 1195–1199.

[3] T. Naito *et al.*, "Beam Oscillation Monitor for the Multi-bunch Beam", in *Proc. IPAC2013*, Shanghai, China, May. 2013, paper MOPME018 , pp. 506–508.

[4] A. Hyvärinen and E. Oja, "Independent Component Analysis: Algorithms and Applications", *Neural Networks*, vol. 13, pp. 411–430, 2000. doi:10.1016/s0893-6080(00)00026-5

[5] F. Laskar, "Frequency analysis for multi-dimensional systems. Global dynamics and diffusion", *Physica D*, vol. 67, pp. 257–281, 1993. doi:10.1016/0167-2789(93)90210-R

[6] A. Langner and R. Tomás, "Optics measurement algorithms and error analysis for the proton energy frontier", *Phys. Rev. ST Accel. Beams*, vol. 18, 031002, 2015. doi:10.1103/PhysRevSTAB.18.031002

[7] Y. Ohnishi, "Highlights from SuperKEKB Commissioning", in *Proc. eeFACT2018*, Hong Kong, China, Sep. 2018, paper MOXAA02, pp. 1–6.

[8] K. Ohmi, The 2018 International Workshop on the High Energy Circular Electron Positron Collider, IHEP, Beijing, China, Nov. 2018. https://indico.ihep.ac.cn/event/7389/